Hindawi
IET Signal Processing
Volume 2023, Article ID 4251265, 16 pages
https://doi.org/10.1049/2023/4251265

Research Article

RF Signal Feature Extraction in Integrated Sensing and Communication

Xiaoya Wang,[1,2] **Songlin Sun**,[1] **Haiying Zhang**,[2] **and Qiang Liu**[3]

[1]*School of Information and Communication Engineering, Beijing University of Posts and Telecommunications, Beijing, China*
[2]*CETC 54th Research Institute, Shijiazhuang, China*
[3]*College of Electronic and Information Engineering, Shandong University of Science and Technology, Qingdao, China*

Correspondence should be addressed to Xiaoya Wang; xy-wang@bupt.edu.cn

Received 23 May 2023; Revised 14 August 2023; Accepted 24 August 2023; Published 28 October 2023

Academic Editor: Sourabh Sahu

Because of the open property of information sharing in integrated sensing and communication, it is inevitable to face security problems such as user information being tampered, eavesdropped, and copied. Radio frequency (RF) individual identification technology is an important means to solve its security problems at present. Whether using machine learning methods or current deep learning-based target fingerprint identification, its performance is based on how well the radio frequency features (RFF) are extracted. Since the received signal is affected by various factors, we believe that we should first find the intrinsic features that can describe the properties of the target, which is the key to enhance the RF fingerprint recognition. In this paper, we try to analyze the intrinsic characteristics of the components that influenced the signal by the transmitting source and derive a mathematical formula to describe the RF characteristics. We propose a method using dynamic wavelet transform and wavelet spectrum (DWTWS) to enhance RFF features. The performance of the proposed method was evaluated by experimental data. Using a support vector machine classifier, the recognition accuracy is 99.6% for 10 individuals at a signal-to-noise ratio (SNR) of 10 dB. In comparison with the dual-tree complex wavelet transform (DT-CWT) feature extraction method and the wavelet scattering transform method, the DWTWS method has increased the interclass distance of different individuals and enhanced the recognition accuracy. The DWTWS method is superior at low SNR, with performance improvements of 53.1% and 10.7% at 0 dB.

1. Introduction

With the continuous development of wireless communication, the next generation of wireless communication systems is expected to achieve radar and communication spectrum sharing, which is called integrated sensing and communication (ISAC). The radar and communication equipment share hardware and spectrum resources in the system [1–4]. Inevitably, there are physical layer security issues, such as the deliberate forgery of user-specific information in the Internet of Vehicles, the easy interception of integrated waveforms by eavesdroppers, and interference between secondary and primary link users when communication and sensing coexist under ISAC. Radio frequency (RF) individual identification technology is currently an important means to address its security issues. RF individual identification technology extracts the inherent characteristics of different chips from the RF signals emitted by transmitting devices [5, 6], thereby obtaining the unique characteristics of each wireless transmitting device to distinguish the identity of wireless communication devices.

The typical RF individual identification process primarily involves receiving data, extracting RF fingerprints, and designing the classifier. Among these, extracting radio frequency features (RFF) is the critical step, and its quality determines the upper limit of machine learning performance [7]. The characteristics used for RFF identification may be transient during data switching or signal start and end [8] or steady state characteristics during normal operation of the radiation source [9, 10]. Current search methods to extract RFF characteristics are divided into model-based, empirical, and data-based methods. The empirical method is the most common one in current applications, which selects physically meaningful or statistically significant parameters as RFF features. These features mainly

include parametric statistical features in the time domain [11–15], parametric statistical features in the frequency domain [16], higher order statistical features [17], and other transformation characteristics. Transformation features such as wavelet [18], Hilbert–Huang's parameter transformation characteristics [19], and parameter decomposition characteristics in empirical mode [20, 21] are more applied. Other features, such as constellation trajectory mapping features [22, 23], fractal dimensional features [24, 25], and multidimensional integrated features, have also been studied more [26–28]. For data-based intelligent processing methods, deep models are used for automatic feature extraction and individual classification and recognition [29–34]. However, the models used are becoming increasingly complex and require very large data samples to train, which are not suitable for application to micromodels or microsystems.

All these methods are valid in physical layer security verification. However, different methods require certain application conditions; some require a high signal-to-noise ratio (SNR) [12, 35], some require good channel quality [36], some completely offline [18, 37], and some use different types of devices [5], and some require large amounts of training data [38, 39].

Amongst these feature extraction algorithms, wavelet processing has good applications in feature extraction, including image processing, spoken word processing, structural damage detection [40], and computer classification and recognition [41] due to its multiple-resolution features and good signal analysis algorithmic capabilities. Almashaqbeh and Klein et al. [36] used dual-tree complex wavelet transform (DT-CWT) on transient signals from Bluetooth devices, extracting features and statistics of wavelet domain signals to create robust fingerprint features with a recognition accuracy of 88% and 80%, respectively. Hou et al. [42] used dynamic wavelet transform to classify the signal for detecting ultrasonic periodontal depth detection using 2D FFT data mapping of wavelet coefficients as tilt indices to achieve detection of periodontal depth with 60% agreement with manual detection for comparison error at 1.5 mm. Choe et al. [43] used the Daubechies-4 wavelet transform combined with an artificial neural network to propose a robust and adaptive device identification system. Li et al. [44] and Zhang et al. [45] also utilized multiscale methods for feature extraction in point cloud segmentation. Ashush et al. [46] used wavelet scattering transform (WST), and CWT approaches to extract RF features and used an unsupervised clustering method to characterize and detect drone swarms.

This article analyses the mechanism of generation of the radiation source based on the idea of multiscale transformation in the wavelet transformation and proposes an individual recognition method based on dynamic small wave transformation and wavelet spectrum (DWTWS). Dynamic wavelet transform and its 2D spectrum decompose transient and steady-state data into different frequency ranges. The amplitude and phase components introduced by "intrinsic deformation" or "extrinsic factors" are separated into different subbands to isolate the RF fingerprint features from the signal [47, 48]. A radial basis function-based support vector machine (SVM) classifier was used. This algorithm can improve security performance without increasing hardware costs. And the processing performance remains good at lower SNR. In terms of complexity, with a CPU main frequency of 1.60 GHz and a memory capacity of 8G Byte, quasi-real-time processing can be achieved, ensuring the application of the algorithm in engineering practice. We used a radial base function SVM classifier to verify the extraction features. In system security certification applications, the algorithm improves recognition performance without increasing hardware costs, and especially at lower SNR, it can still maintain good performance. In terms of complexity, in the CPU's main frequency is 1.60 GHz, and the storage capacity is 8G Byte; it can realize the real-time processing and ensure the application of the algorithm in engineering practice.

The main contributions of this paper are as follows:

(1) Modeling and analyzing the nonlinear fingerprint features of the signals from the RF signal generation mechanism analyzed the factors affecting individual characteristics and gave the formula that affects the characteristics.
(2) In this article, we propose a new method DWTWS to extract the characteristics of individual signals. This method can effectively extract the amplitude changes and phase change information in the signal and build a distinctive feature space with obvious differences. Discusses the performance of DWTWS on nonlinear fingerprint characteristics.
(3) The proposed features can be used as a preprocessing step of some existing networks, which are used for target individual recognition, signal classification, and image segmentation. Performance improvement was verified by experiments.
(4) We experimented with the characteristic formulas proposed in this article under different SNRs. Compared with traditional methods, the methods of this article can get better.

2. Mechanism of RF Feature Generation

The proposed feature extraction algorithm for the dynamic wavelet transform and wavelet spectrum (DWTWS) includes three parts—RF feature generation mechanism, signal feature extraction, and signal classifier. In Section 2, we first introduce the RF feature generation mechanism and describe the impact of the three main nonlinear components in RF signal generation—equivalent filters, oscillators, and amplifiers. We derive the representation of DWTWS features. And we obtained a representation of the inherent attribute features of the individual. We then provide a flowchart for DWTWS processing in Section 3. A and designs a 24D feature of DWTWS, forming feature vectors to represent individuals. We also give a graph of the characteristics of different individuals. In Section 4, individual recognition experiments based on DWTWS 24D features are described,

and the experimental performance under different conditions is provided.

2.1. Model of Signal Generation. The digital modulated signal is modeled as Equation (1).

$$\begin{aligned} S_{\mathrm{m}}(t) &= \left[\sum_k x_k g(t - kT_s - \tau)\right] e^{j(\omega_c t + \theta_0)} \\ &= m(t) e^{j(\omega_c t + \theta_0)}, \end{aligned} \tag{1}$$

$$m(t) = \sum_k x_k g(t - kT_s - \tau), \tag{2}$$

where $S_{\mathrm{m}}(t)$ is the modulated signal, and $m(t)$ is the modulated signal, x_k is the information sequence, $g(t)$ is the impulse response of the shaped filter with pulse width T_s, ω_c is the carrier angular frequency, θ_0 is the initial phase, and τ is the time delay.

The major active components through which the modulated signal passes from generating the information sequence, modulating the signal generation, and then transmitting it from the antenna include mixers, RF filters, and amplifiers. The nonideal characteristics of these active devices affect the RF signal and produce a slight deviation from the ideal performance. These stable, recurring characteristics form the inherent RFF characteristics of the device.

2.2. Factors Affecting Signal Fingerprinting. The modulated signal has to pass through an RF filter after changing to intermediate frequency (IF) by the mixer. Its major role is to allow the eligible signal to pass and suppress the undesired frequency signal. The filter needs to be consistent with the frequency and bandwidth of the RF signal to achieve the above functional. Also, the subtle features of the filter impact the passing RF signal, including filter amplitude skew or ripple in the frequency response and changes in group delay. Equation (3) gives its time domain representation.

$$S_{\mathrm{m}}(t) = \left[m(t) e^{j(\omega_c t + \theta_0)}\right] \times h_0(t), \tag{3}$$

where $h_0(t)$ is the impulse response of the ideal filter with flat amplitude and continuous phase in the pass-band. $h(t)$ denotes the filter impulse response with subtle features, and the filter distortion consists mainly of amplitude distortion and phase distortion, which represents in the frequency domain as Equation (4) [22, 49].

$$H(f) = H_0(f) A(f) \epsilon^{j\varphi(f)}, \tag{4}$$

$$A(f) \doteq a_0 + a_n \cos(2\pi\alpha_n f), \tag{5}$$

$$\varphi(f) \doteq 2\pi b_0 f + b_n \sin(2\pi\beta_n f), \tag{6}$$

where a_0 and b_0 are the linear gain, a_n and b_n are the gain of amplitude and phase fluctuations, α_n and β_n are fluctuating period. In practical applications, α_n and β_n may be consist of multiple components. Here, we use first-order coefficients and ignore higher order coefficients. Since it is smaller and produces a smaller effect.

The amplitude $A(f)$ distortion adds a pair of derivative waveforms to the filter. The phase $\varphi(f)$ distortion affects the amplitude and time delay of the filter and introduces a complex set of derivative waveforms. The effect of filter aberrations is similar to the summation of multiple path delays, which can be illustrate in Equation (7) [22].

$$\begin{aligned} h(t) = {} & J_0(b_n) h_0(t + b_0) + J_1(b_n) h_0\left(t + b_0 + n/B_\varphi\right) - h_0\left(t + b_0 - n/B_\varphi\right) \\ & + \frac{a_n}{2} \begin{pmatrix} J_0(b_n) h_0(t + b_0 + n/B_A) + J_1(b_n) \\ h_0\left(t + b_0 + n/B_A + n/B_\varphi\right) - h_0\left(t + b_0 + n/B_A - n/B_\varphi\right) \end{pmatrix} \\ & + \frac{a_n}{2} \begin{pmatrix} J_0(b_n) h_0(t + b_0 - n/B_A) + \\ J_1(b_n) h_0\left(t + b_0 - n/B_A + n/B_\varphi\right) - h_0\left(t + b_0 - n/B_A - n/B_\varphi\right) \end{pmatrix}, \end{aligned} \tag{7}$$

where $J_0(\cdot)$ denotes the zero-order Bessel function and $J_1(\cdot)$ denotes the first-order Bessel function.

From the above formula, it can be seen that the influence of the nonideal characteristics of the filter in signal generation can be reflected in the high-order terms of the amplitude and phase of the output signal.

Wavelet transform can decompose signals into different frequency bands for analysis, analyze the instantaneous characteristics of signals, and have multiresolution characteristics for different frequencies. It can effectively extract unique information in special frequency bands of signals. At the same time, wavelet transform also has high time and frequency resolution, high computational efficiency, and is suitable for real-time signal processing. So, we choose wavelet transform for extracting RF fingerprint features.

The nonideal properties of the filter, acting on the RF signal, are depicted as shown in Equation (3), and its wavelet transform is represented in Equation (8).

$$W_f(a, b) = < m(t) e^{j(\omega_c t + \theta_0 + \varphi_0(t))} \times h_0(t), \psi_a(t - b) > . \tag{8}$$

The 2D Fourier transform is a transformation of the wavelet coefficients from the spatial domain to the frequency domain, reflecting the details and variations in the wavelet

coefficients. The detailed part is usually shown in the high-frequency component. There are also peaks reflected in the 2D Fourier transform for the components of regularity in the wavelet coefficients. The Fourier transform of the wavelet coefficients from the signal going through the distortion filter is expressed in Equation (9).

$$FT\{W_f(a,b)\} = \frac{\sqrt{a}}{2} e^{j\theta_0} M(\omega-\omega_c) H_0(f) A(f) e^{j\varphi(f)} e^{-\pi^2 f_b (af-f_c)^2}. \tag{9}$$

When the scale of wavelet coefficients is taken a_k such that $a_k f_k = f_c$, the value of wavelet coefficients is maximum and contains the information of the k th mode. When the analysis is performed in the complex frequency domain, the amplitude and phase spectra for $a_k f_k = f_c$ are as follows:

$$FT\{W_f(a_k,b)\} = \frac{\sqrt{\alpha_\kappa}}{2} e^{j\theta_0} |M(f-f_c))\|H_0(f)\|A(f)| \times e^{j\varphi M^f e^{j\varphi}(f)} e^{-\pi^2 f_b (af-fc)^2}, \tag{10}$$

$$\left|W_{a_k,b}(f)\right| = \frac{\sqrt{\alpha}}{2} |M(f-f_c)||H_0(f)||A(f)|, \tag{11}$$

$$\varphi_{a_k,b}(f) = \varphi_M(f) + \varphi_\alpha(f) + \varphi(f) + \theta_0, \tag{12}$$

$$|A(f)| = a_0 + \frac{a_n}{2}\left(e^{j2\pi\alpha_n f_k} + e^{-j2\pi\alpha_n f_k}\right), \tag{13}$$

$$\varphi_\alpha(f) = J_0(b_n) + \sum_{i=1}^{\infty} J_i(b_n)\left(e^{j(i2\pi\beta_n f)} + (-1)^i e^{-j(i2\pi\beta_n f)}\right). \tag{14}$$

The oscillator is a nonlinear system with feedback, and its main index is frequency stability. The main impact of its nonideality on the generated RF signal is shown in the small phase jitter on the carrier frequency [22, 50, 51], which is expressed as $\varphi_0(t)$ here. RF signal of modulated signal with oscillator phase jitter is expressed as follows:

$$S_{\mathrm{m}}(t) = m(t) e^{j(\omega_c t + \theta_0 + \varphi_0(t))}, \tag{15}$$

where $\varphi_0(t) = (1-c_0)\varphi_0(t-1) + c_0 N(t)$, $N(t)$ is Gaussian white noise, and c_0 varies with individual differences.

Bringing the RF signal obtained from Equation (15) into the equation of wavelet transform to obtain the representation of its wavelet coefficients in Equation (16).

$$W_0(a,b) = <m(t) e^{j(\omega_c t + \theta_0 + \varphi_0(t))}, \psi_a(t-b)>, \tag{16}$$

$$\psi_a(t-b) = \frac{1}{\sqrt{f_b \pi}} e^{\frac{j2\pi f_c (t-b)}{a}} e^{-\frac{(t-b)^2}{a^2 f_b}}. \tag{17}$$

The wavelet coefficients are in complex form. It contains the information of the kth mode. We can obtain their largest value when the scale of the wavelet coefficients is a_k, such that $a_k f_k = f_c$. Equation (18) gives its representation in the form of amplitude and phases. $W_0(a_k, b)$ represents its amplitude and $\varphi_o(b)$ represents its phase.

$$W_0(a_k,b) = |W_0(a_k,b)| e^{j\varphi_0(b)}, \tag{18}$$

$$|W_0(a_k,b)| = \frac{\sqrt{\alpha_\kappa}}{2} \sum_k x_k g(b - kT_s - \tau), \tag{19}$$

$$\varphi_0(b) = \arg(W_0(a_k,b)) = 2\pi a_k f_k b + \psi(b) + \theta_0. \tag{20}$$

Phase features $\psi(b)$ can be found in the phase of wavelet coefficients, reflecting the effects generated by the nonlinear oscillator.

The RF signal passes through an amplifier to amplify the voltage/power of the signal before it enters the antenna. The amplifier is compressed in the saturation region to produce an amplitude modulation to amplitude modulation (AM–AM) effect; that is, the amplitude will produce compression; amplitude modulation to phase modulation (AM–PM) effects occur in the unsaturated region, i.e., phase changes are produced [49, 22]. We can express the effect of the amplifier on the signal in terms of the Taylor series, see Equation (21). It can be seen that the amplitude variation of the second term is excessive to the signal, producing an additional phase.

$$S_{\mathrm{m}}(t) = \lambda_1\left[m(t) e^{j(\omega_c t + \theta_0)}\right] + \sum_{k=2}^{K} \lambda_{2k-1} |m(t)|^{2k} m(t) e^{j(\omega_c t + \theta_0)}, \tag{21}$$

where λ_1 and λ_{2k-1} are the coefficients of the Taylor series. λ_{2k-1} decreases as k increases. Its value becomes small when k is above the 2nd order, usually $\lambda_1 = 1$, $\lambda_3 < 0$. When λ_1 is a real number, it causes the amplitude compression of the signal $S_{\mathrm{m}}(t)$, resulting in the AM–AM effect. When it is a complex number, it causes the phase distortion of the signal $S_{\mathrm{m}}(t)$, i.e., the AM–PM effect.

The wavelet transform of the distorted signal caused by the nonideal characteristics of the amplifier is described in Equation (22).

$$W_A(a,b) = \frac{\sqrt{\alpha}}{2} \lambda_1 \sum_k x_k g(b - kT_s - \tau) e^{jv\pi f_c b} e^{-\pi^2 f_b (af-fc)^2} + \frac{\sqrt{\alpha}}{2} \sum_{n=2}^{N} \lambda_{2k-1} |\Sigma_k x_k g(b - kT_s - \tau)|^{2k+1} \times e^{j(2\pi f_c b + \theta_0)} e^{-\pi^2 f_b (af-fc)^2}. \tag{22}$$

When $a_k f_k = f_c$, the largest value of the wavelet transform coefficients is obtained and it is given by Equation (23).

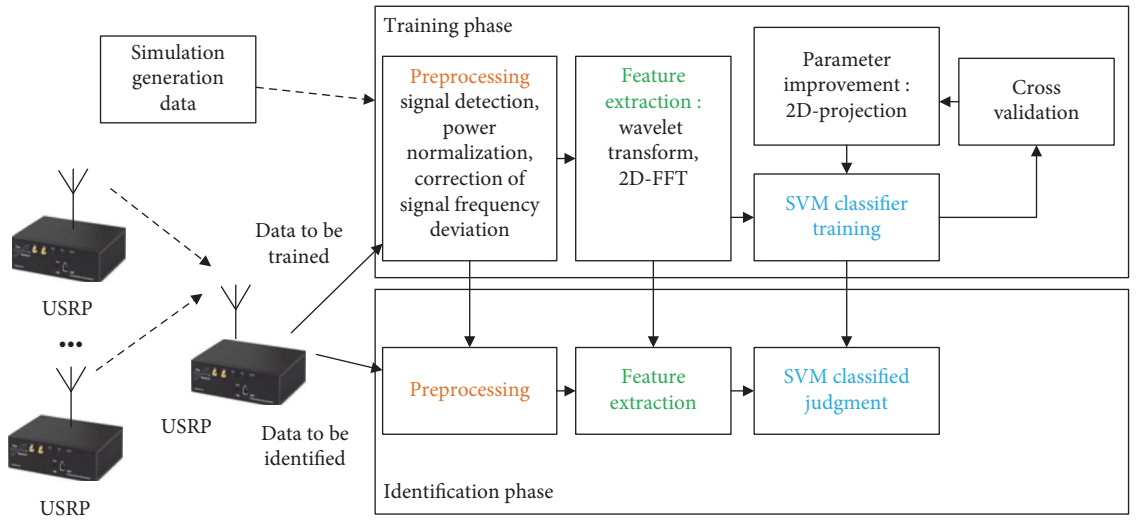

FIGURE 1: Overall architecture for signal collection, analysis signal generation, fingerprint extraction, and classification.

$$W_A(a_k,b)=\frac{\sqrt{\alpha_k}}{2}\lambda_1\sum_k x_k g(b-kT_s-\tau)e^{j2\pi f_c b}e^{j\theta_0}e^{-\pi^2 f_b(a_k f-fc)^2}+\frac{\sqrt{\alpha_k}}{2}\sum_{n=2}^{N}\lambda_{2k-1}|\Sigma_k x_k g(b-kT_s-\tau)|^{2k+1}\times e^{j(2\pi f_c b+\theta_0)}e^{-\pi^2 f_b(a_k f-fc)^2}, \tag{23}$$

$$|W_A(a_k,b)|=\frac{\sqrt{a_k}}{2}\lambda_1\sum_k x_k g(b-kT_s-\tau)+\frac{\sqrt{a_k}}{2}\sum_{n=2}^{N}\lambda_{2k-1}\left|\sum_k x_k g(b-kT_s-\tau)\right|^{2k+1}, \tag{24}$$

$$\varphi_A(b)=2\pi f_c b+\theta_0. \tag{25}$$

3. Approach

3.1. Overall Architecture. All results presented in Section 4 are generated by the overall demonstration process shown in Figure 1. The main hardware and software processes are given in Figure 1. It mainly includes three parts: signal acquisition and generation, training stage, and recognition stage. The data collection process involves two types: (1) simulation generation and (2) free-space signal collection using multiple USRP N210s from Ettus Research as the transmitter sources and one USRP N210 as the receiver. Saves the signal from the transmitter source as text files, each containing millions of lines of data. The collected signal data (a series of complex samples) are passed to postprocessing, which is done in a MATLAB 2018b environment.

The first type of data are used for verification of the feature extraction and classification, and the second is conducted for the performance comparison test.

The training phase includes preprocessing of signal detection, feature extraction, parameter enhancement, and classifier design. The processing of each part in the recognition and training stages is similar. The implementation and functions of the individual processes in Figure 1 are discussed in the following sections.

3.2. Preprocessing for Feature Extraction. Good classification performance relies on the uniqueness, robustness, and repeatability of the features. Otherwise, it cannot be achieved if the underlying features vary greatly during the signal processing interval. In real engineering applications, the receiver and transmitter can be in different places and distances during two receptions. The emitting antennas may have dissimilar efficiencies and gains at different times. The amplitude of the same individual varies considerably. To avoid the effects caused by these factors, the received signal must be preprocessed to reduce the adverse effects of external interference. Besides, the different magnitudes of different features have different ranges of values. It may cause an extensive range of gradients in the network, and there may be a gradient explosion and gradient disappearance, resulting in network instability. Normalization of the feature data is also required.

Preprocessing includes signal detection, power normalization, and correction of signal frequency deviation. Signal detection is to determine the starting point of the RF signal. We use a double sliding window approach to detect the location of the signal appearance, using a change point detection algorithm to find abrupt changes in the signal and determine the location of the signal, avoiding the noisy part of the original signal from corrupting our RF signature. Power normalization is performed by dividing the processed data by the largest module. The frequency bias is measured by Chirp Z-transform and corrected.

3.3. Feature Extraction. To ensure that the selected feature set has the desired fingerprint properties while reducing noise interference, it should have the following characteristics:

(1) Reduced size to reduce processing and storage requirements.

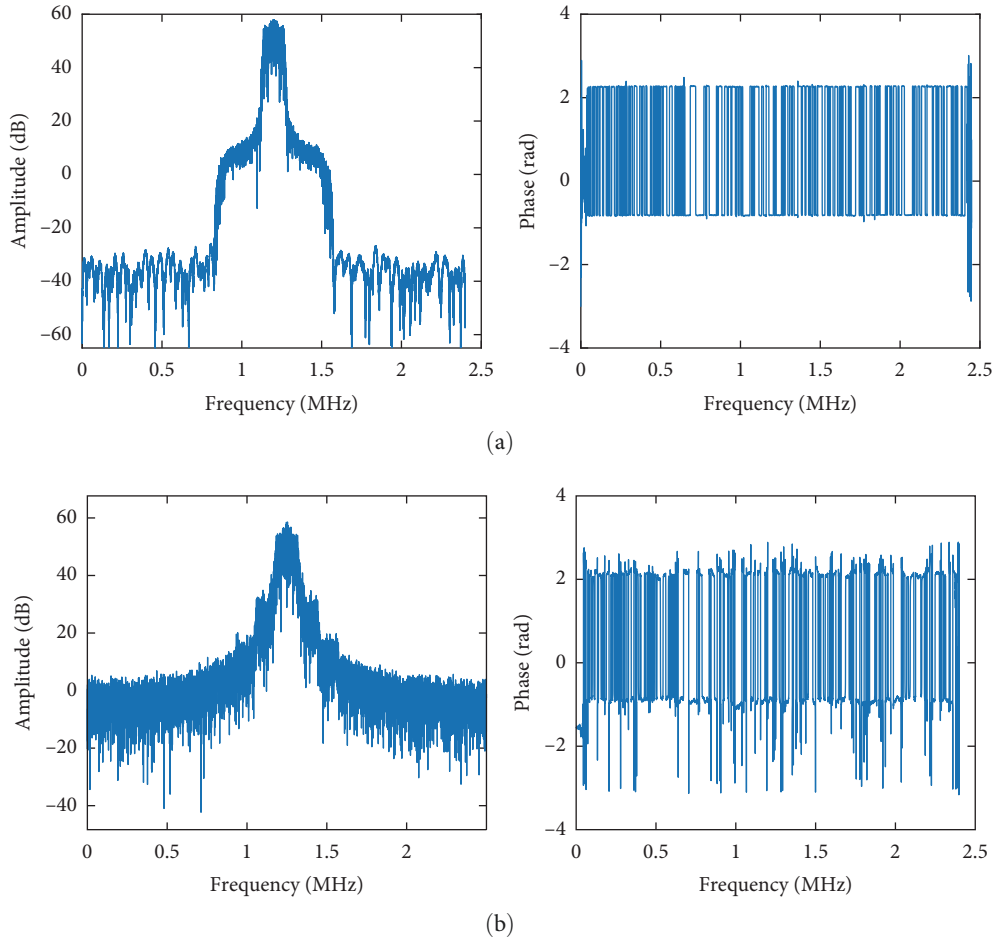

Figure 2: Amplitude spectrum (after shifting) and phase spectrum of signals. (a) Amplitude spectrum (after shifting) and phase spectrum of ideal signal. (b) Amplitude spectrum (after shifting) and phase spectrum of signal through the combined distortion of the three nonlinear devices.

(2) Intradevice repeatability.

(3) Interdevice uniqueness.

Based on the analysis in Section 2, the preprocessed data were divided into multiple time segments. A wavelet transform was performed for each segment using a complex Morlet wavelet (cmor1–0.1) as wavelet bases. The dynamic transformation coefficients of the wavelets are projected on the time-scale axis, a 2D projection, in slices of thickness H, that is 0.25. The 2D projection is subjected to a 2D Fourier transform to get its amplitude and phase spectrum.

From the above analysis, it can be seen that the influence of the civic characteristics of the filter, oscillator, and amplifier on the RF-modulated signal is mainly reflected in the amplitude and phase of the signal. Those wavelet coefficients and the wavelet spectrum are used as the 4D basic features for classification and recognition.

The problem of I/Q modulation imbalance for quadrature modulation, described in the literature [22], can be represented in the amplitude and phase distortion of the signal, which does not require special processing. Such an impact on the amplitude and phase spectra is specified in Figure 2. The upper two figures in Figure 2 give the amplitude spectrum and phase spectrum of the ideal signal. Figure 2 shows the amplitude spectrum (after shifting) and phase spectrum of the distorted signal with parameters {0.01, 1, 0.0415, 0, 0.0228, 4;4, 1, $-0.16-j^*$ 0.02, $0.02+j^*$ 0.01}.

Compared to the amplitude and phase spectra of the ideal signal, the nonideal signal has an elevated noise floor in the signal amplitude spectrum, a large burr in the phase spectrum at the sign jump point, and a phase jitter during the sign duration. The larger the parameters, the more significant the perturbation to the carrier frequency.

As a multiresolution analysis method, wavelet transform can characterize the local features of signals in both time and frequency domains [52]. It is an efficient method of extracting critical information on dynamic signals and is a pivotal technique for automatic signal classification applications.

Wavelet transform has multiresolution characteristics. The dynamic wavelet transform uses the relevant characteristics of time series. This correlation characteristic can be expressed through the 2D Fourier transform. The projection of different frequency slices can show different detailed features and periodic components in the wavelet coefficients.

It can be used as a feature quantity together with the dynamic wavelet coefficients to distinguish different individual signals.

Figure 3 shows the 2D projection of the dynamic wavelet coefficients and the slice of its 2D Fourier transform at a specific frequency of the signal after these three nonlinear devices. Figure 3(a) shows the 2D projection of the dynamic wavelet coefficients of the signal after it passes through the three nonlinear models with parameter 0.02. It should be noted here that the horizontal axis of the wavelet coefficients is the pseudo-time domain coordinates. In order to correspond with the time domain waveform, we use time′ here. The upper half of the two plots in Figure 3(b) shows the 0.95–1.15 ms portion of the time domain signal waveform. The left panel is a zoomed-in view of the red box in Figure 3 (a), and the right panel is a zoomed-in view of the 2D projection of the wavelet coefficients of the signal through the filter model with parameter 0.005. Comparing the wavelet coefficients with different parameters, they are more representative of the different detailed features during the symbol duration. Figure 3(c) shows the slices of the 2D Fourier transform of the wavelet coefficients at 1.125 MHz (corresponding to a scale of 30 for the wavelet coefficients) after two parametric models as follows:

- parameters for the left panel: $\{c_0, a_0, a_n, b_0, b_n, \alpha_n; \beta_n, \lambda_0, \lambda_3, \lambda_5\} = \{$ 0.02, 1, 0.0415, 0, 0.0228, 3; 3, 1, −0.16 $-j^*$ 0.02, 0.02 $+ j^*$ 0.01$\}$
- parameters for the right panel: $\{c_0, a_0, a_n, b_0, b_n, \alpha_n; \beta_n, \lambda_0, \lambda_3, \lambda_5\} = \{$0.005, 1, −0.0218, 0, −7e-4, 4, 4,1, −0.24 $-j^*$ 0.03, 0.03 $+ j^*$ 0.01$\}$.

Directly using the magnitude and phase of wavelet coefficients and those of their 2D spectrum as features for classification can be prohibitive in terms of data storage and computational processing time. By reducing the dimensionality of the feature space used for device classification, the computational burden can be reduced. This approach has been used in some literatures, for example [35, 36], where the statistical properties inherent in the underlying signal features can be used for device classification. The statistics include mean (μ_x, 1D feature), variance (σ_x^2, 2D attribute), skewness (γ_x, 3D characteristic), and kurtosis (κ_x, 4D feature), which are outlined in Equations (26)–(29).

$$\mu_x = \frac{1}{N_x}\sum_{k=1}^{N_x}[x(k)], \tag{26}$$

$$\sigma_x^2 = \frac{1}{N_x}\sum_{k=1}^{N_x}[x(k)-\mu_x]^2, \tag{27}$$

$$\gamma_x = \frac{1}{\sigma_x^3 N_x}\sum_{k=1}^{N_x}[x(k)-\mu_x]^3, \tag{28}$$

$$\kappa_x = \frac{1}{\sigma_x^4 N_x}\sum_{k=1}^{N_x}[x(k)-\mu_x]^4, \tag{29}$$

where N_x denotes the number of data sample points. $x(k)$ denotes the magnitude and phase of the wavelet coefficients and those of their 2D spectra, respectively. The flow of fingerprint feature extraction is shown in Figure 4.

The preprocessed data are read and parsed, including signal detection, data segmentation, data normalization, and frequency correction. The wavelet transform and the Fourier transform are calculated using Equations (10)–(25) to get two types of basic features, whose statistical classification features are calculated using Equations (26)–(29). The resulting fingerprint features (feature vector) for each burst consist of 24D features (2 types of data × 2 types of features × 4 statistical features). The fingerprint features from device c can be given by Equation (30).

$$\begin{aligned} F_{wd}^c = [&\mu_{wd}(a), \mu_{wd}(\phi), \mu_{Fwd}(a), \mu_{Fwd}(\phi),\\ &\sigma_{wd}^2(a), \sigma_{wd}^2(\phi), \sigma_{Fwd}^2(a), \sigma_{Fwd}^2(\phi),\\ &\gamma_{wd}(a), \gamma_{wd}(\phi), \gamma_{Fwd}(a), \gamma_{Fwd}(\phi),\\ &\kappa_{wd}(a), \kappa_{wd}(\phi), \kappa_{Fwd}(a), \kappa_{Fwd}(\phi)], \end{aligned} \tag{30}$$

where $c = 1, 2, \ldots, 10$ is the number of classes of the device. $\mu_\cdot(\cdot)$ is the mean of statistical features (1D feature). $\sigma_\cdot^2(\cdot)$ is the variance of statistical features, the 2D attribute of statistical features. $\gamma_\cdot(\cdot)$ is the skewness, the 3D characteristic of statistical features. $\kappa_\cdot(\cdot)$ is the kurtosis (the 4D feature) of statistical features. The subscript wd denotes the feature of the wavelet transform, while Fwd denotes the feature of the 2D Fourier transform. a is the feature of the obtained signal amplitude, and φ is the feature of the obtained signal phase.

Combining these is represented as follows:

$\mu_{wd}(a)$ refers to the statistical average characteristics of the amplitude after wavelet transform.

$\kappa_{wd}(\varphi)$ and $\kappa_{Fwd}(\varphi)$ refers to the kurtosis of the phase after wavelet transform and 2D Fourier transform.

Other variables have similar meanings. It is reasonable to compare the behavior of different devices using a given technique and a given token. In this case, cross-device differences indicate potential discriminability, and larger differences correspond to increased category divisibility using classifier processing.

3.4. Classifier Design. In this article, we use a one-to-many SVM classifier, which has many unique advantages in small sample resolution, nonlinear and high-dimensional pattern recognition, and use the Gaussian radial basis function as the kernel function, which significantly improves the SVM classifier's performance. The kernel function converts the vector transformation into the inner product operation between vectors and maps the original feature vectors to the high-dimensional feature space. Ultimately, the linear distinction between multiclass individuals is reached.

Experiments were conducted on 10 ($c = 10$) different devices, with 1,000 gusts of data per device. A total of 24D feature vectors, the statistics of the magnitude and phases of wavelet coefficients and those of their 2D spectrum, are used as inputs to the SVM classifier. The 1,000 fingerprint vectors for each apparatus form a composite fingerprint matrix, whose size is 24,000.

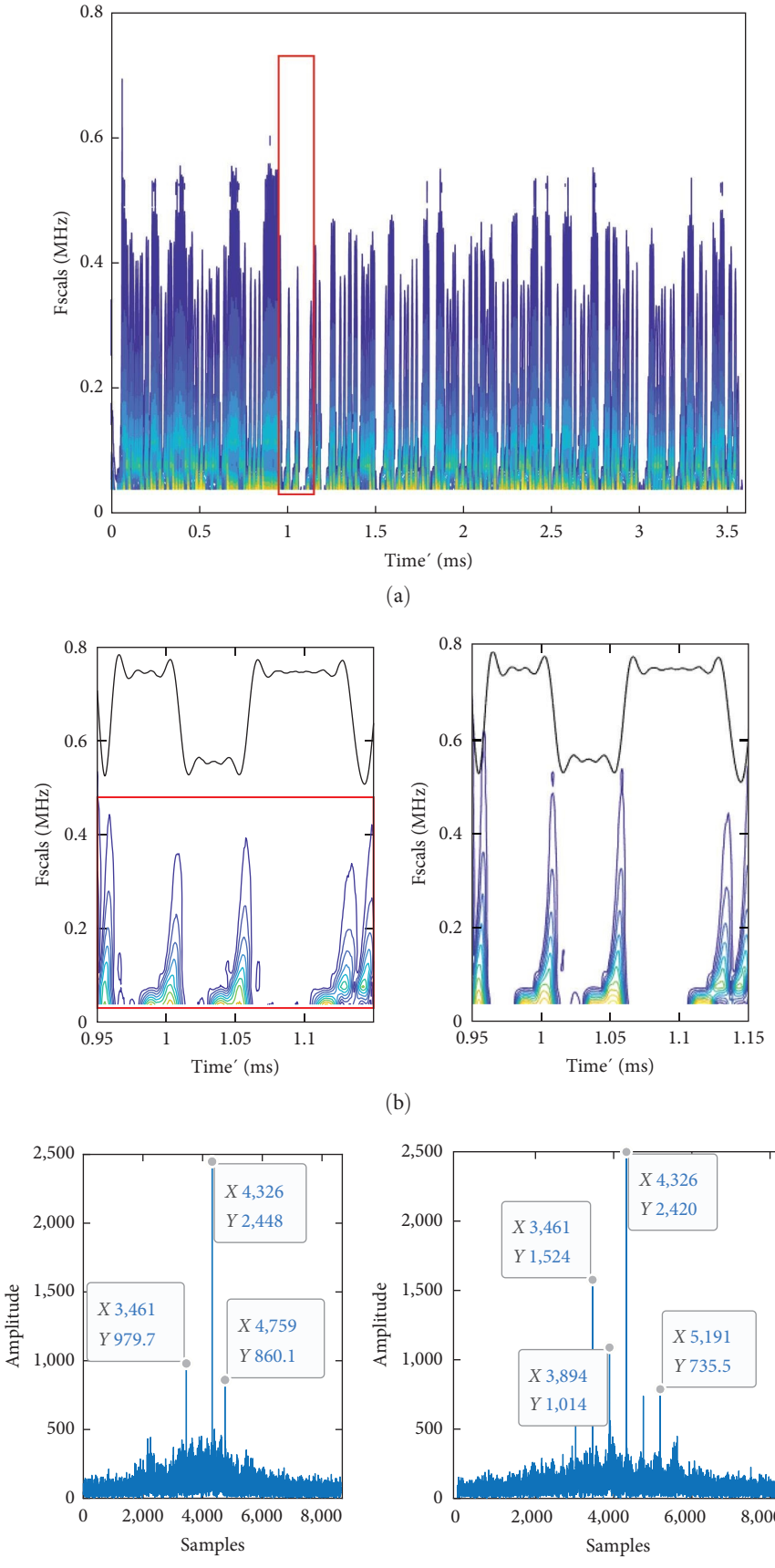

FIGURE 3: 2D projections of the dynamic wavelet coefficients of the signal passing through two different sets of parametric models and the slices of their 2D Fourier transform at a specific frequency. (a) 2D projection of the dynamic wavelet coefficients of the distorted signal. (b) The left panel is a zoom-in of the graph in red box of (a), and the right panel is a local zoom-in of the wavelet coefficients of the distorted signal with different parameters. (c) Slices of the 2D Fourier transform of the wavelet coefficients at a frequency of 1.125 MHz of the signal through different parametric models.

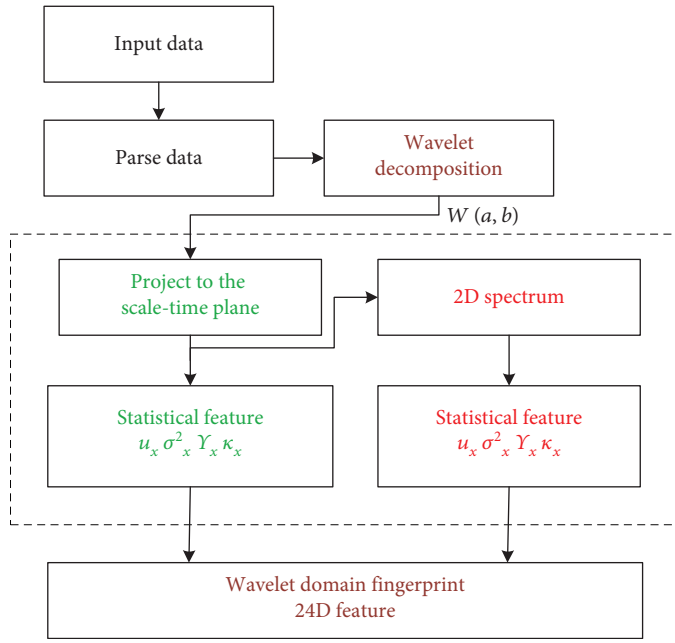

Figure 4: Flowchart of feature extraction.

As seen in Figure 5, Di ($i = 1,\ldots, k$) is the ith block of the input data. Monte Carlo and k-fold cross-validation methodologies were used for individual identification tests. The Monte Carlo method ensures statistical significance, and the k-fold cross-validation method was used to generalize predictive errors to independent datasets. Empirically consider a total of NMC times (NMC = 50) independent Monte Carlo noise realizations. Based on experience, k was selected for 5 and 10. When the experimental k was 5, the recognition accuracy was 0.01% lower than that of 10, and the recognition time was 5% shorter. In this article, the experiments were used to verify the effectiveness of features, k was selected as 5, while considering the engineering applications in microsystems. The 1,000 pulses from each device were divided into five equal subsets (200 each), of which four subsets (800 fingerprints) were used for training and the remaining "reserved" subset (200 fingerprints) was used for classification. Similar to the literature [41], Figure 5 shows a detailed process for k-fold cross-validation. Note that the fold iteration accumulator in Figure 5 is cleared prior to the beginning of each iteration.

Training fingerprints used for SVM and posttraining decision limits are calculated from the ML distribution. The subsequent comparison of the performance of various methods in the paper is the accuracy comparison of classification recognition with the same confidence interval. The confidence interval (CI) is chosen as CI = 95% [41] and is computed as Equation (31).

$$\mathrm{CI} = \pm 1.96 \sqrt{\frac{p(1-p)}{N_p}}, \tag{31}$$

where p is the correct ratio computed by dividing the number of correct classifications by N_p, the number of tests. All

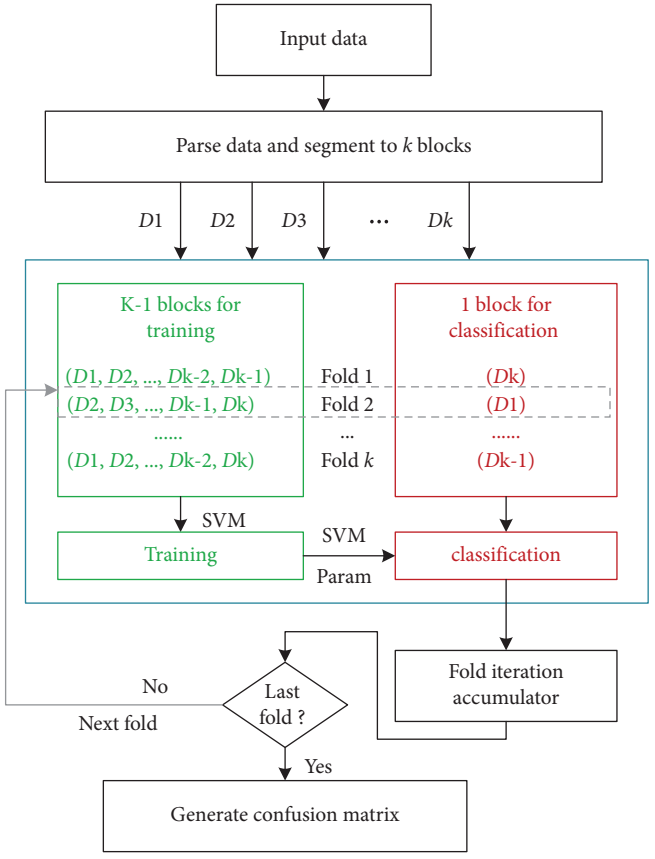

Figure 5: Classification process of K-fold cross-validation.

results for subsequent experiments in the article were generated using 1,000 bursts per device and performed Monte Carlo iterations of the 50 (NMC = 50) SVM process. Thus, there is a total of 50,000 ($N_p = 1{,}000 \times 50$) independent

classification decisions per device, i.e., the percentage of each row of the SVM classification confusion matrix is based on 50,000 trials.

4. Experiments

4.1. Device Classification Based on Dynamic Wavelet Transform. The data collection process involves two types: simulation generation and free-space signal collection using multiple USRP N210s. The collection data were acquired using USRP N210s as transmitting and receiving devices. The modulation style is binary phase shift keying, with a symbol rate of 120-kiloBaud.

The first type of data is simulated and generated through the addition of different parameters to the acquired data. First, the USRP is used as the transmitter to acquire RF data and generate zero IF IQ data. Second, different oscillator, filter, and amplifier parameter models are synthesized with the acquired I/Q data. Different individuals' RF data are generated. The three sets of test parameters are selected as follows:

- $\{c_0, a_0, a_n, b_0, b_n, \alpha_n; \beta_n, \lambda_0, \lambda_3, \lambda_5\} = \{0.01, 1, 0.0415, 0, 0.0228, 4; 4, 1, -0.16 - j^* 0.02, 0.02 + j^* 0.01\}$;
- $\{c_0, a_0, a_n, b_0, b_n, \alpha_n; \beta_n, \lambda_0, \lambda_3, \lambda_5\} = \{0.02, 1, 0.0228, 0, 0.0007, 4; 4, 1, -0.24 - j^* 0.03, 0.03 + j^* 0.01\}$;
- $\{c_0, a_0, a_n, b_0, b_n, \alpha_n; \beta_n, \lambda_0, \lambda_3, \lambda_5\} = \{0.05, 1, 0.0622, 0, -0.007, 4; 4, 1, -0.08 - j^* 0.06, 0.03 + j^* 0.03\}$.

The second type of data was collected in a controlled outdoor environment, and the entire collection period lasted over 1 week. The data was collected using 11 USRP N210s of the same model, 10 as emitting sources and 1 as receiving device, to generate data for 10 individuals.

The RF frequency is 1 GHz, the sampling rate (representing by F_s) is 2.4 Mega samples per second, and the sampling interval (representing by T_s) is reciprocal of the sampling rate, i.e. $T_s = 1/F_s \approx 416.67$ nanoseconds. The RF signal is down-converted to zero IF to get I/Q data, which is done in the flowing processing. The typical SNR of the acquired signal is 30 decibels (dB). Each burst contains 200 symbols of the same preamble and 4,800 loading symbols.

The original sample data contains 1,000 bursts, and the data samples of each individual generated after passing three sets of parameters still contain 1,000 bursts. Of these, 800 burst samples were used for training, and the remaining 200 were used for testing. The three individual data were preprocessed using the method of Section 3.2, the characteristic data were obtained as the process of Figure 4 in Section 3.3, and classification tests are performed using the SVM classifier in Section 3.4. The three groups of individuals generated by the simulation were identified with an accuracy rate of 99.9% at an SNR of 30 dB. Figure 6 gives a 2D scatter plot of the mean wavelet coefficient phase versus the mean spectral amplitude of the wavelet coefficient spectral.

The following is an individual identification test of data collected by 10 USRP transmitter devices to verify the recognition performance of the DWTWS algorithm under

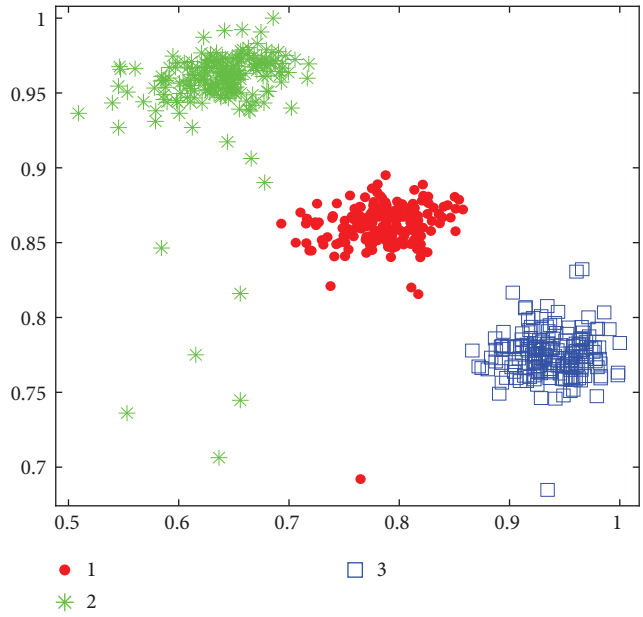

FIGURE 6: 2D scatter plot of the mean of wavelet coefficient phase versus the kurtosis of wavelet spectrum with different parameters at 30 dB SNR.

different SNRs. For the 10 individual data collected, the Monte Carlo method was used to add noise to achieve the SNR required for analysis. Noise data is generated by using Matlab software to first obtain a Gaussian distribution of random complexes and then filtered by a digital filter with the same bandwidth as the signal. The noise data are then appropriately scaled and superimposed onto different individual data, resulting in different noise-added samples with different SNRs.

As with the simulation data, 1,000 burst sample data were used for each type of individual. Of these, 800 burst samples were used for training, and the remaining 200 were used for testing. The correct classification and identification rate for 10 types of devices is 99.8% when the SNR of the data is 30 dB. Figure 7 gives a confusion matrix for the recognition of 10 device classifications, recall rate (the table on the right side of the confusion matrix), and precision (the table at the bottom of the confusion matrix chart) table of 10 devices identified at 30 dB SNR. It shows the sensitivity to changes in different individuals, where categories 4 and 10, as well as categories 6 and 8, are less distinguished and prone to confusion. Use the column and row summaries to display precision and recall rates for each class. The table at the bottom of the confusion matrix table shows the precision values. The table on the right side shows the recall values.

We can realize that these characteristics are not the same for different individuals, as shown in Figure 8. It gives a 2D scatter plot of 10 individuals of the mean phase of the wavelet coefficient versus the mean spectral amplitude. Some individuals have large intervals in characteristics, and some gaps are small, which are related to the performance differences of devices in equipment manufacturing.

The identification model trained from the original acquisition data and the sample data under different SNRs are

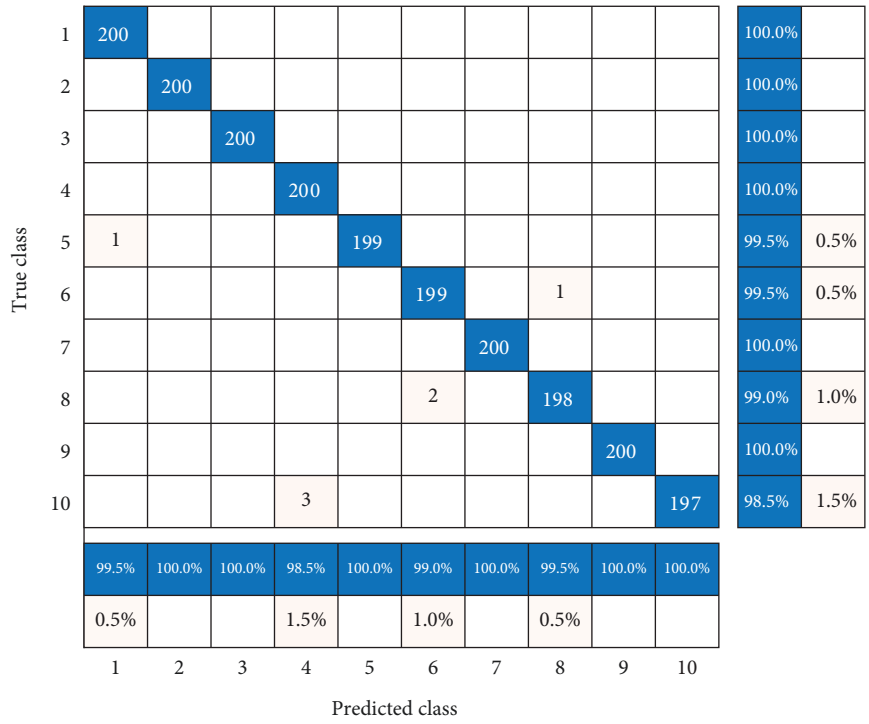

Figure 7: Confusion matrix, recall rate (the table on the right side of the confusion matrix), and precision (the table at the bottom of the confusion matrix chart) table of 10 devices identified at 30 dB SNR.

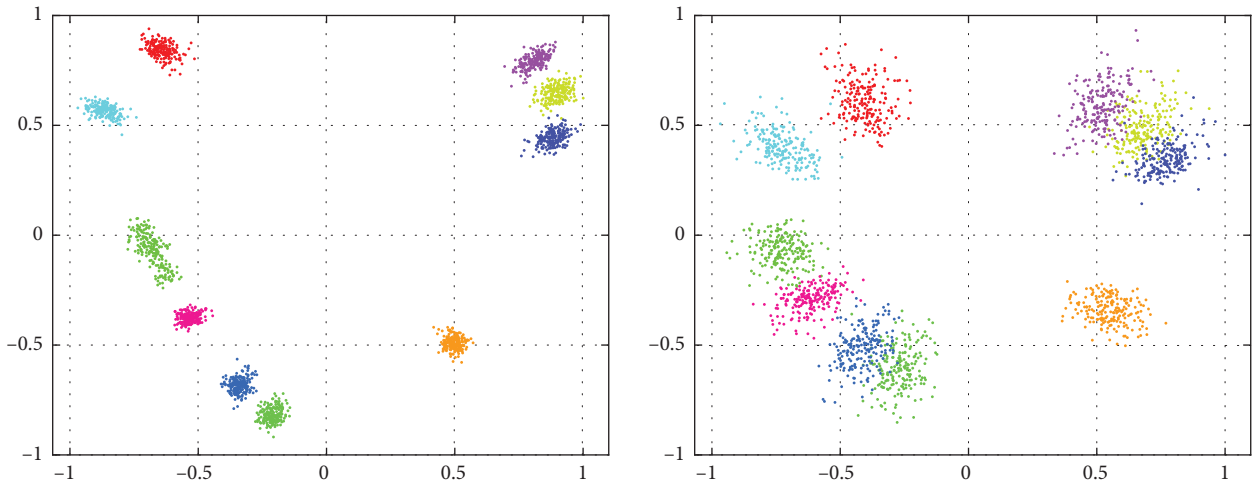

Figure 8: 2D scatter plot of the mean of wavelet coefficient phase vs. the kurtosis of wavelet spectrum of 10 individuals. The left image shows 10 dB, while the right shows 0 dB.

selected for the identification experiments. They are carried out on the SNR from 0 to 30 dB, the commonly used environment in communication. We use the DWTWS algorithm and the DT-CWT algorithm in [36] and the WST algorithm in the literature [10] for experimental comparison. The DT-CWT algorithm is a typical application of wavelet transform in extracting signal fingerprint features. The literature [10] used CWT, DWT, and wavelet time scattering transform (WST) for feature extraction, respectively, with the best performance of the WST algorithm. This paper conducted a comparison test using 672D features obtained after WST decomposition and SVM classifier.

Table 1 gives the recognition accuracy of the three algorithms at 0–30 dB SNR. Figure 9 shows the comparison curves of the three algorithms. When SNR is greater than 20 dB, the performance of the three algorithms does not differ much, and the correct recognition rates are 99.92%, 98.50%, and 95.40%, respectively. The DWTWS algorithm shows better performance at a low SNR of 0–15 dB. It can be found that the DWTWS algorithm is less affected when the

Table 1: Recognition accuracy (%) of three algorithms.

SNR (dB)	DWTWS algorithm in this paper (%)	DT-CWT algorithm in the literature [36] (%)	WST algorithm in the literature [10] (%)
30	99.93	99.60	97.30
25	99.92	99.30	96.40
20	99.92	98.50	95.40
15	99.80	93.90	94.50
10	99.60	83.00	92.50
5	99.30	59.00	90.50
0	96.40	33.30	85.70
−5	88.30	15.71	73.80

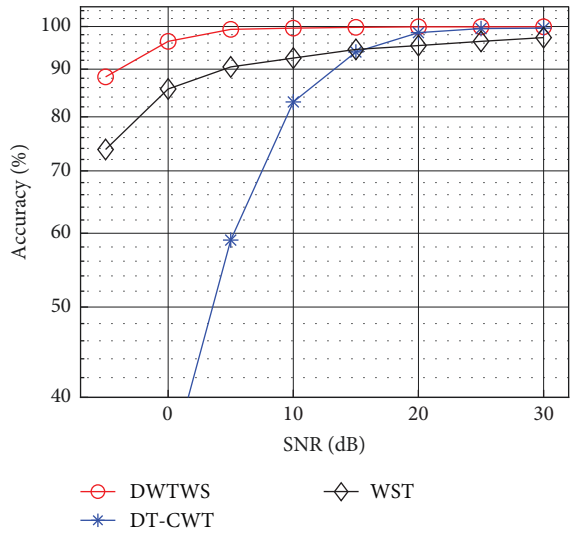

Figure 9: Recognition accuracy curves of three algorithms at −5–30 dB SNR.

SNR is reduced. For example, when the SNR is 10 dB, the recognition accuracy of the DWTWS algorithm remains at 99.60%, that of the DT-CWT algorithm drops to 83.00%, and that of the WST algorithm is 90.5%. When the SNR is 0 dB, the recognition accuracy of the DWTWS algorithm is 96.4%, that of the DT-CWT algorithm drops to 33.3%, and that of the WST algorithm is 85.7%. The recognition accuracy of the DWTWS algorithm is 53.1% and 10.7% higher than those two, respectively.

It can be seen from the test results that with the reduction of the SNR, the reduction in DWTWS and WST algorithms is not significant. The sensitivity of the features proposed in this article to noise is not significant. The SNR has less influence on the DWTWS feature, which has great value for applications under a low SNR environment. The test results also verified the correctness of the analysis in Section 2. This is because the subtle change information of the phase and amplitude better reflects the specific information of the RF circuit.

4.2. Expanded Individual Size Test. In order to verify the generalization performance of the DWTWS algorithm, another eight USRP individuals were collected under the same conditions. Tests were performed to obtain the recognition accuracy under the conditions of −5−30 dB SNR when the total number of RF individuals was increased to 18.

After training using the new data, the DWTWS feature extraction algorithm can still achieve recognition accuracy of 95.3% at an SNR of 10 dB and 89.3% at 0 dB. The DT-CWT method in the literature [36] has a recognition accuracy of 70.8% at an SNR of 10 dB, which rapidly decreases to 23.9% at 0 dB. The WST method in the literature [10] has a recognition accuracy of 89.4% at 10 dB SNR and 81.7% at 0 dB, as shown in Figure 10. Figure 11 gives the 2D plot of wavelet coefficients phase and wavelet spectral kurtosis plot of the DWTWS algorithm of 18 individuals at 10 dB SNR. It can be seen that as the number of categories increases, the accuracy of recognition will decrease. However, the interclass distance between different individuals is still large. Thus, the generalizability of the DWTWS feature extraction algorithm in this paper is further confirmed.

4.3. Computational Complexity Analysis. When individual identification is applied in the field of wireless communication, the complexity of its algorithm is also a key consideration. The following is an analysis of the complexity of the processing process.

It linearly related the preprocessing complexity to the amount of data, i.e., $O(N)$, where N is the number of data points. Wavelet transform also has a complexity of $O(N\log N)$. From the definition of the wavelet transform, there is no integration and differentiation, but only multiplication and addition, which matches perfectly with the instructions of modern computers. The running time of 2D FFT is $O(M^*N\log(M^*N))$, where M is the scale maximum. The time complexity of finding the mean and variance is both $O(N)$ and that of kurtosis and skewness is $O(N)$. Then, the stepwise calculation of the processing required in the flowchart to derive the signal characteristics is $O(N\log N) + 5^* O(N) + O(M^* N\log(M^* N))$. According to statistical theory, the computational complexity depends mainly on $O(M^* N\log(M^* N))$ when N is large.

Table 2 gives the complexity of the DWTWS algorithm, the DT-CWT algorithm [36], and the WST algorithm [10] under the same conditions. The DT-CWT algorithm only completes the calculation of wavelet transform and statistical features, which have low complexity. The WST algorithm

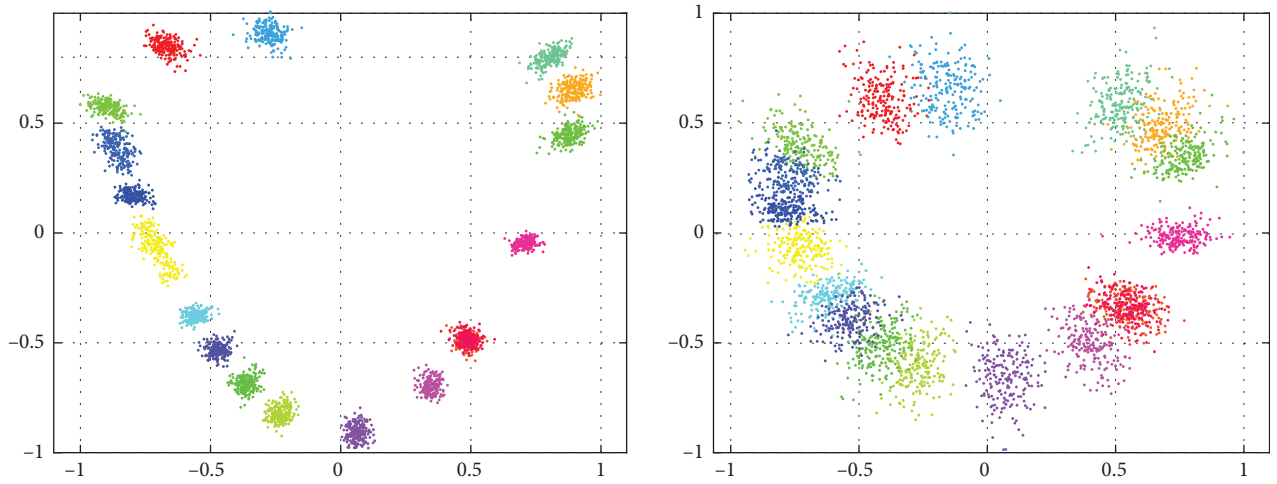

Figure 10: 2D plot of wavelet coefficients phase and wavelet spectral kurtosis plot of DWTWS algorithm of 18 individuals. The left image shows 10 dB, while the right shows 0 dB.

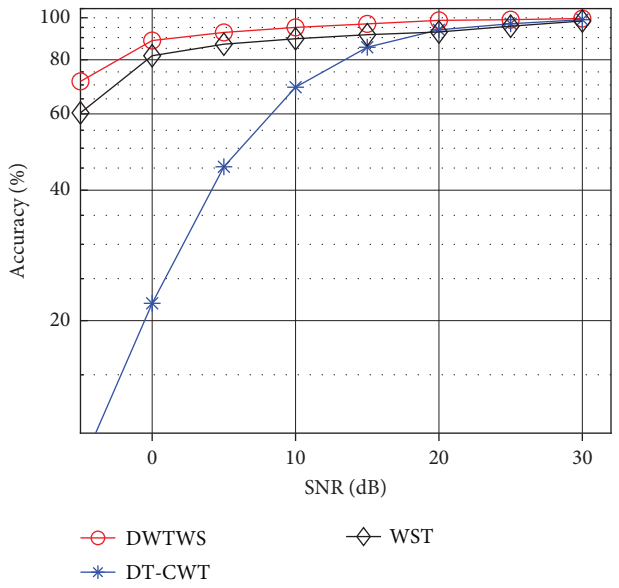

Figure 11: Recognition accuracy curves of three algorithms for 18 devices at −5–30 dB SNR.

Table 2: Comparison of the complexity of three algorithms.

DWTWS algorithm in this paper	DT-CWT algorithm in the literature [36]	WST algorithm in the literature [10]
$O(M^*N\log(M^*N))$	$O(N\log(N)+N)$	$O(L^*N\log(N)+LN)$

N is the number of sampling points and M is the maximum scale of wavelet transform. L is the number of layers.

computes multilayer wavelet transformation, nonlinear mode, and averaging operation, while the DWTWS algorithm includes wavelet transformation and 2D FFT operation, both with similar complexity.

5. Conclusion and Future Work

Based on the security issues in ISAC, we analyzed the influence of different composition components from the principle of radiation source composition, and we presented DWTWS, the statistics of wavelet coefficients, and wavelet spectra after dynamic wavelet transforms as RF fingerprint features. These features have scaling invariant, translation invariant, and rotation invariant features, which can be well adapted to the situation where the radiation source orientation changes and the distance changes. The experiment on 18 radiation source individuals' datasets proves that it can show obvious performance advantages over the traditional algorithm DT-CWT and WST in the 35 dB wide SNR range of −5–30 dB. In the case of low SNR, the advantage of DWTWS features is

more pronounced. This feature extraction algorithm can be used in RF personal identification technology to solve security issues in current wireless networks. Moreover, this feature extraction machine learning method is also suitable for use in microsystems and microprocessor devices due to its limited demand for hardware devices.

In the field of signal processing, the signal reception may be affected by external interference, fading, and other environments. DWTWS features are characterized by low sensitivity and strong robustness and can be used for preprocessing in signal target individual recognition, signal classification, image recognition, and other fields. This feature extraction algorithm is particularly suitable for use in microsystems and microprocessor devices. Under the premise of ensuring performance, it can be achieved using limited resources, avoiding the need for a large number of resources and computational power in modern intelligent models.

Subsequent research will increase the use of the mutual correlation of information and develop a pretraining model for rating characteristics and analyzing the importance of signal characteristics. Meanwhile, further research will be conducted to extract the signal characteristics of the long-term accumulated data. Discern the stability of the attributes over a wide time range and determine the characterization performance of being proposed. Further research will also be pursued to study the mechanism of radiation source fingerprint generation, establish a much more complete mathematical model, and improve the interpretability and identification capability of RF individual identification in engineering applications.

Data Availability

The data are collected based on USRP and are currently private and cannot be publicly downloaded.

Conflicts of Interest

The authors declare that they have no conflicts of interest.

Acknowledgments

This study was funded on the horizontal cooperation projects research funding.

References

[1] F. Liu, Y. Cui, C. Masouros et al., "Integrated sensing and communications: toward dual-functional wireless networks for 6G and beyond," *IEEE Journal on Selected Areas in Communications*, vol. 40, no. 6, pp. 1728–1767, 2022.

[2] R. Zhang, X. Jing, S. Wu, C. Jiang, J. Mu, and F. R. Yu, "Device-free wireless sensing for human detection: the deep learning perspective," *IEEE Internet of Things Journal*, vol. 8, no. 4, pp. 2517–2539, 2021.

[3] R. Zhang, C. Jiang, S. Wu, Q. Zhou, X. Jing, and J. Mu, "Wi-Fi sensing for joint gesture recognition and human identification from few samples in human–computer interaction," *IEEE Journal on Selected Areas in Communications*, vol. 40, no. 7, pp. 2193–2205, 2022.

[4] Y. Cui, F. Liu, X. Jing, and J. Mu, "Integrating sensing and communications for ubiquitous IoT: applications, trends, and challenges," *IEEE Network*, vol. 35, no. 5, pp. 158–167, 2021.

[5] H. Almashaqbeh, Y. Dalveren, and A. Kara, "A study on the performance evaluation of wavelet decomposition in transient-based radio frequency fingerprinting of Bluetooth devices," *Microwave and Optical Technology Letters*, vol. 64, no. 4, pp. 643–649, 2022.

[6] A. C. Polak, S. Dolatshahi, and D. L. Goeckel, "Identifying wireless users via transmitter imperfections," *IEEE Journal on Selected Areas in Communications*, vol. 29, no. 7, pp. 1469–1479, 2011.

[7] M. J. Rana, M. S. Alam, and M. S. Islam, "Continuous wavelet transform based analysis of low frequency oscillation in power system," in *2015 International Conference on Advances in Electrical Engineering (ICAEE)*, pp. 320–323, IEEE, Dhaka, Bangladesh, December 2015.

[8] A. M. Ali, E. Uzundurukan, and A. Kara, "Improvements on transient signal detection for RF fingerprinting," in *2017 25th Signal Processing and Communications Applications Conference (SIU)*, pp. 1–4, IEEE, Antalya, Turkey, May 2017.

[9] D. Zanetti, B. Danevs, and S. Capkun, "Physical-layer identification of UHF RFID tags," in *Proceedings of the sixteenth annual international conference on Mobile computing and networking*, pp. 353–364, Association for Computing Machinery, New York, NY, USA, September 2010.

[10] O. O. Medaiyese, M. Ezuma, A. P. Lauf, and I. Guvenc, "Wavelet transform analytics for RF-based UAV detection and identification system using machine learning," *Pervasive and Mobile Computing*, vol. 82, Article ID 101569, 2022.

[11] M. G. Frei and I. Osorio, "Intrinsic time-scale decomposition: time–frequency–energy analysis and real-time filtering of non-stationary signals," *Proceedings of the Royal Society A: Mathematical, Physical and Engineering Sciences*, vol. 463, no. 2078, pp. 321–342, 2007.

[12] K. Bonne Rasmussen and S. Capkun, "Implications of radio fingerprinting on the security of sensor networks," in *2007 Third International Conference on Security and Privacy in Communications Networks and the Workshops - SecureComm 2007*, pp. 331–340, IEEE, Nice, France, September 2007.

[13] Q. Tian, Y. Lin, X. Guo, J. Wang, O. AlFarraj, and A. Tolba, "An identity authentication method of a MIoT device based on radio frequency (RF) fingerprint technology," *Sensors*, vol. 20, no. 4, Article ID 1213, 2020.

[14] S. Sobot, V. Ninkovic, D. Vukobratovic, M. Pavlovic, and M. Radovanovic, "Machine learning methods for device identification using wireless fingerprinting," in *2022 International Balkan Conference on Communications and Networking (BalkanCom)*, pp. 183–188, IEEE, Sarajevo, Bosnia and Herzegovina, August 2022.

[15] N. Wang, W. Li, L. Jiao, A. Alipour-Fanid, T. Xiang, and K. Zeng, "Orientation and channel-independent RF fingerprinting for 5G IEEE 802.11ad devices," *IEEE Internet of Things Journal*, vol. 9, no. 11, pp. 9036–9048, 2022.

[16] J. Han, C. Qian, P. Yang et al., "GenePrint: generic and accurate physical-layer identification for UHF RFID tags," *IEEE/ACM Transactions on Networking*, vol. 24, no. 2, pp. 846–858, 2016.

[17] A. Abdelaziz, C. E. Koksal, R. Burton et al., "Beyond PKI: enhanced authentication in vehicular networks via MIMO," in *2018 IEEE 19th International Workshop on Signal Processing Advances in Wireless Communications (SPAWC)*, pp. 1–5, IEEE, Kalamata, Greece, June 2018.

[18] C. A. Miller and M. K. Hinders, "Classification of RFID tags with wavelet fingerprinting," in *Intelligent Feature Selection for Machine Learning Using the Dynamic Wavelet Fingerprint*, pp. 207–246, Springer, Cham, 2020.

[19] N. E. Huang, Z. Shen, S. R. Long et al., "The empirical mode decomposition and the Hilbert spectrum for nonlinear and non-stationary time series analysis," *Proceedings of the Royal Society of London. Series A: Mathematical, Physical and Engineering Sciences*, vol. 454, no. 1971, pp. 903–995, 1998.

[20] J. Wei, L. Yu, L. Zhu, and X. Zhou, "RF fingerprint extraction method based on CEEMDAN and multidomain joint entropy," *Wireless Communications & Mobile Computing*, vol. 2022, Article ID 5326892, 16 pages, 2022.

[21] S. Deng, Z. Huang, X. Wang, and G. Huang, "Radio frequency fingerprint extraction based on multidimension permutation entropy," *International Journal of Antennas and Propagation*, vol. 2017, Article ID 1538728, 6 pages, 2017.

[22] Y. Pan, S. Yang, H. Peng, T. Li, and W. Wang, "Specific emitter identification using signal trajectory image," *Journal of Electronics & Information Technology*, vol. 42, no. 4, pp. 941–949, 2020.

[23] Y. Li, Y. Ding, J. Zhang, G. Goussetis, and S. K. Podilchak, "Radio frequency fingerprinting exploiting non-linear memory effect," *IEEE Transactions on Cognitive Communications and Networking*, vol. 8, no. 4, pp. 1618–1631, 2022.

[24] Y. Huang and H. Zheng, "Radio frequency fingerprinting based on the constellation errors," in *2012 18th Asia-Pacific Conference on Communications (APCC)*, pp. 900–905, IEEE, Jeju, Korea (South), October 2012.

[25] G. Huang, Y. Yuan, X. Wang, and Z. Huang, "Specific emitter identification based on nonlinear dynamical characteristics," *Canadian Journal of Electrical and Computer Engineering*, vol. 39, no. 1, pp. 34–41, 2016.

[26] L.-Z. Qu, H. Liu, K.-J. Huang, and J.-A. Yang, "Specific emitter identification based on multi-domain feature fusion and integrated learning," *Symmetry*, vol. 13, no. 8, Article ID 1481, 2021.

[27] S. Guo, R. E. White, and M. Low, "A comparison study of radar emitter identification based on signal transients," in *2018 IEEE Radar Conference (RadarConf18)*, pp. 286–291, IEEE, Oklahoma City, OK, USA, April 2018.

[28] Y. Xing, A. Hu, J. Zhang, J. Yu, G. Li, and T. Wang, "Design of a robust radio-frequency fingerprint identification scheme for multimode LFM radar," *IEEE Internet of Things Journal*, vol. 7, no. 10, pp. 10581–10593, 2020.

[29] Y. Wang, G. Gui, Y. Lin, H.-C. Wu, C. Yuen, and F. Adachi, "Few-shot specific emitter identification via deep metric ensemble learning," *IEEE Internet of Things Journal*, vol. 9, no. 24, pp. 24980–24994, 2022.

[30] H. Parmaksız and C. Karakuzu, "A review of recent developments on secure authentication using RF fingerprints techniques," *Sakarya University Journal of Computer and Information Sciences*, vol. 5, no. 3, pp. 278–303, 2022.

[31] W. Wu, S. Hu, Y. Gao, and J. Cao, "Federated learning based distributed algorithms for RF fingerprinting extraction and identification of IoT devices," in *Artificial Intelligence for Communications and Networks*, vol. part I 3, pp. 3–18, Springer International Publishing, Springer, Cham, 2021.

[32] Q. Wu, C. Feres, D. Kuzmenko et al., "Deep learning based RF fingerprinting for device identification and wireless security," *Electronics Letters*, vol. 54, no. 24, pp. 1405–1407, 2018.

[33] M. Liu, J. Wang, N. Zhao, Y. Chen, H. Song, and F. R. Yu, "Radio frequency fingerprint collaborative intelligent identification using incremental learning," *IEEE Transactions on Network Science and Engineering*, vol. 9, no. 5, pp. 3222–3233, 2022.

[34] M. Liu, Z. Yan, and J. Zhang, "Energy and spectrum efficient radio frequency fingerprint intelligent blind identification," in *2022 IEEE 95th Vehicular Technology Conference: (VTC2022-Spring)*, pp. 1–5, IEEE, Helsinki, Finland, June 2022.

[35] C. Bertoncini, K. Rudd, B. Nousain, and M. Hinders, "Wavelet fingerprinting of radio-frequency identification (RFID) tags," *IEEE Transactions on Industrial Electronics*, vol. 59, no. 12, pp. 4843–4850, 2012.

[36] R. W. Klein, M. A. Temple, and M. J. Mendenhall, "Application of wavelet-based RF fingerprinting to enhance wireless network security," *Journal of Communications and Networks*, vol. 11, no. 6, pp. 544–555, 2009.

[37] Y. Shen, J. Xu, J. Yi, E. Chen, and V. Chen, "Class-E power amplifiers incorporating fingerprint augmentation with combinatorial security primitives for machine-learning-based authentication in 65 nm CMOS," *IEEE Transactions on Circuits and Systems I: Regular Papers*, vol. 69, no. 5, pp. 1896–1909, 2022.

[38] V. Brik, S. Banerjee, M. Gruteser, and S. Oh, "Wireless device identification with radiometric signatures," in *Proceedings of the 14th ACM international conference on Mobile computing and networking*, pp. 116–127, Association for Computing Machinery, New York, NY, USA, September 2008.

[39] T. Morehouse and R. Zhou, "RF device identification using CNN based PUF," in *2020 IEEE 63rd International Midwest Symposium on Circuits and Systems (MWSCAS)*, pp. 217–220, IEEE, Springfield, MA, USA, August 2020.

[40] J. Hou, *Ultrasonic Signal Detection and Recognition Using Dynamic Wavelet Fingerprints*, The College of William and Mary, 2004.

[41] A. Grinsted, J. C. Moore, and S. Jevrejeva, "Application of the cross wavelet transform and wavelet coherence to geophysical time series," *Nonlinear Processes in Geophysics*, vol. 11, no. 5/6, pp. 561–566, 2004.

[42] J. Hou, S. T. Rose, and M. K. Hinders, "Ultrasonic periodontal probing based on the dynamic wavelet fingerprint," *EURASIP Journal on Advances in Signal Processing*, vol. 2005, Article ID 198348, 2005.

[43] H. C. Choe, C. E. Poole, A. M. Yu, and H. H. Szu, "Novel identification of intercepted signals from unknown radio transmitters," *Wavelet Applications II. SPIE*, vol. 2491, pp. 504–517, 1995.

[44] D. Li, G. Shi, Y. Wu, Y. Yang, and M. Zhao, "Multi-scale neighborhood feature extraction and aggregation for point cloud segmentation," *IEEE Transactions on Circuits and Systems for Video Technology*, vol. 31, no. 6, pp. 2175–2191, 2021.

[45] J. Zhang, Q. Su, B. Tang, C. Wang, and Y. Li, "DPSNet: multitask learning using geometry reasoning for scene depth and semantics," *IEEE Transactions on Neural Networks and Learning Systems*, vol. 34, no. 6, pp. 2710–2721, 2023.

[46] N. Ashush, S. Greenberg, E. Manor, and Y. Ben-Shimol, "Unsupervised drones swarm characterization using RF signals analysis and machine learning methods," *Sensors*, vol. 23, no. 3, Article ID 1589, 2023.

[47] W. Wang, Z. Sun, S. Piao, B. Zhu, and K. Ren, "Wireless physical-layer identification: modeling and validation," *IEEE Transactions on Information Forensics and Security*, vol. 11, no. 9, pp. 2091–2106, 2016.

[48] S. Elakkiya and S. Audithan, "Feature based object recognition using discrete wavelet transform," in *Second International*

Conference on Current Trends In Engineering and Technology - ICCTET 2014, pp. 393–396, IEEE, Coimbatore, India, July 2014.

[49] Agilent Technologies, "Agilent technologies wireless test solutions application note 1313," in *Testing and Troubleshooting Digital RF Communications Transmitter Designs*, Agilent Technologies, 2000.

[50] G. Sridharan, *Phase Noise in Multi-Carrier Systems*, pp. 9–44, University of Toronto (Canada), 2010.

[51] N. Soltanieh, Y. Norouzi, Y. Yang, and N. C. Karmakar, "A review of radio frequency fingerprinting techniques," *IEEE Journal of Radio Frequency Identification*, vol. 4, no. 3, pp. 222–233, 2020.

[52] R. X. Gao and R. Yan, *Wavelets: Theory and Applications for Manufacturing*, Springer Science & Business Media, 2010.